Fusion Engineering and Design xxx (2009) xxx–xxx

Contents lists available at ScienceDirect

Fusion Engineering and Design

journal homepage: www.elsevier.com/locate/fusengdes

Multipurpose ANSYS FE procedure for welding processes simulation

Andrea Capriccioli, Paolo Frosi*

ENEA CR Frascati, Via Enrico Fermi 45, 00044 Frascati, Italy

ARTICLE INFO

Article history:
Available online xxx

Keywords:
Finite element method
Welding
Birth and death

ABSTRACT

ANSYS FE procedures and 3D models for thermal and mechanical simulation of both Laser and TIG welding processes are presented. The special features are the applicability to a non uniform gap and the use of a fast iterative procedure that assures the constancy of the fixed maximum temperature along the single pass and between each pass and the following, apart from their shapes and sizes. All the thermal and mechanical material properties of both INCONEL 625 and AISI 316 are described till to liquid phase; convection and radiation effects are considered. The 3D ANSYS models use both brick and non linear contact elements and elastic and elastic–plastic materials.

Two full simulation are presented: a laser welding test (taken from ENEA) and a TIG welding one (source W7-X) with the root seam plus 14 passes; thermal and mechanical results are reported in the two cases and for the latter an extensive sensitivity analysis, changing mesh size of the filling material, welding speed and material properties, is explained with results and comparisons. This large sensitivity analysis has been executed for TIG welding because in this case (multi-pass welding) the reduction of CPU time is a strong requirement; but some conclusions are helpful for laser welding too. The mechanical calculation results very sensitive to the mesh shape: this fact implies very fine and regular meshes. The specimens are first restrained and then welded with the foreseen welding procedure; after that it is released and the final linear and angular shrinkages are calculated. The ANSYS birth and death procedure is used and the CPU time was strongly reduced.

1. Introduction

This report is a presentation of ANSYS FE models for the thermal and mechanical welding simulation. To develop suitable welding numerical models, we must consider the process parameter (welding speed, number and sequence of passes, filling material supplying, etc.), the geometrical constraints, the material nonlinearities and all physical phenomena involved in welding. Therefore it is a great challenge to consider all factors at the same time; so generally the models include some approximations: in the works [1–6] we can find some attempts to reduce modeling efforts and computer time.

The present work deals with the following main assumptions and features about the thermal model:

a) the displacements of the parts, during the welding, do not affect the thermal distribution of the parts themselves;
b) all the material properties are described till to the liquid phase of metal;
c) convection and radiation effects are considered;
d) both Laser and TIG methodologies for root and/or filling weld are modeled;
e) the ANSYS element birth and death procedure is used;

The thermal analysis is the first step and during this phase the distributions of the temperatures are calculated and saved for every load step. We assume that the thermal calculation at a given time is independent from the structural results obtained at a previous time according to the point (a): so the thermal and the mechanical analysis can be uncoupled.

2. Thermal analysis

At about 1650 K the material is melted and over this value we have liquid. The AISI 316 thermal material properties (taken from the ITER database) are reported in Tables 1 and 2. We can't know from this database the same data in the liquid phase: so the only way at this stage of the analysis is to keep constant the physical properties outside the solid range. Besides we have used the enthalpy ($\Delta H = \int \rho(T)c(T)\mathrm{d}T$): this function can be constructed from the previous values of density (ρ) and specific heat (c) at the same temperature; the arbitrary constant coming from the integration has been defined equal to the product ρcT at 0 °C. Then at the "*solidus*" temperature (1643 K) we have added the latent heat

* Corresponding author. Tel.: +39 06 94005837; fax: +39 06 94005147.
E-mail address: frosi@frascati.enea.it (P. Frosi).

0920-3796/$ – see front matter © 2009 Elsevier B.V. All rights reserved.
doi:10.1016/j.fusengdes.2009.01.039

Table 1
AISI 316 thermal material property.

Temperature (K)	Density (kg/m^3)	Scecific heat (J/kg K)	Thermal conductivity (W/m K)	Enthalpy (J/m^3)
273	8038.70	456.28	13.29	9.76E+08
293	8030.47	464.73	13.63	1.05E+09
373	7997.02	494.23	14.99	1.35E+09
473	7954.03	522.74	16.62	1.75E+09
573	7909.76	543.92	18.19	2.16E+09
673	7864.18	559.87	19.72	2.59E+09
773	7817.31	572.69	21.26	3.03E+09
873	7769.13	584.49	22.81	3.48E+09
973	7719.66	597.38	24.42	3.94E+09
1073	7668.90	613.45	26.09	4.41E+09
1173	7616.83	634.82	27.86	4.90E+09
1273	7563.47	663.58	29.76	5.40E+09
1373	7508.81	701.85	31.81	5.93E+09
1473	7452.85	751.72	34.03	6.49E+09
1573	7395.60	815.30	36.46	7.09E+09
1643	7354.75	869.09	38.29	7.54E+09

to obtain the enthalpy value at the "*liquidus*" temperature (1673 K): so we model with only one material parameter the whole "thermal history" including heat exchange during solidification or melting. In the liquid phase we have kept constant c and ρ, so the enthalpy in that range has a constant slope given by the last values defined for c and ρ (Fig. 1).

In Fig. 2 we can see a laser fem model: the zone near the caulker has been modeled with a finer mesh while the rear zone has been modeled with a coarser one; the two zones are tied together with contact elements (conta173 and targe170) using the option "multi-point-constraint". The heat source movement has been simulated with a thermal load applied to the elements that represent the fused material at a given time: that is a "column" of elements at the bottom of caulker has been loaded at every load step.

The birth and death technique has been used: in the case of laser welding the elements describing the molten material (the central ones at the bottom of caulker) are kept "live" during the thermal analysis because they really absorbed the heat energy. Then at the beginning of mechanical analysis the same elements are "killed" to

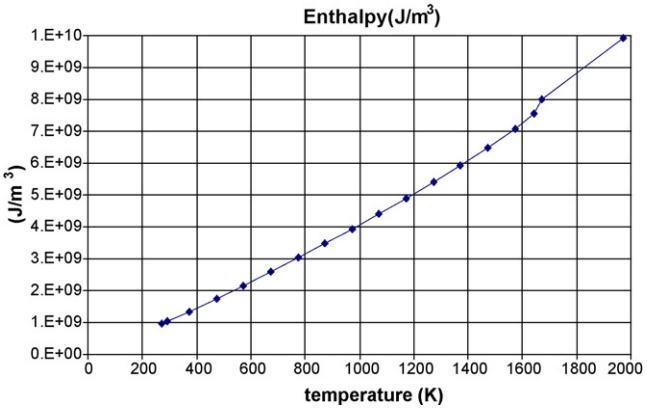

Fig. 1. Graph of enthalpy for AISI 316.

Table 2
INCONEL 625 thermal material property.

Temperature (K)	Temperature (°C)	Thermal conductivity (W/m K)	Density (kg/m^3)	Specific heat (J/kg K)	Enthalpy (J/m^3)
273	0	9.64	8446	405.5	934984869
293	20	9.8991	8440	410.36	1.004E+09
323	50	10.292	8430.7	417.65	1.109E+09
373	100	10.958	8414.6	429.8	1.287E+09
423	150	11.637	8398.3	441.95	1.47E+09
473	200	12.33	8381.8	454.1	1.658E+09
523	250	13.038	8365.3	466.25	1.851E+09
573	300	13.758	8348.7	478.4	2.048E+09
623	350	14.493	8331.9	490.55	2.25E+09
673	400	15.242	8314.6	502.7	2.457E+09
723	450	16.004	8296.9	514.85	2.668E+09
773	500	16.78	8278.6	527	2.884E+09
823	550	17.57	8259.9	539.15	3.104E+09
873	600	18.374	8211.3	551.3	3.329E+09
923	650	19.191	8162.7	563.45	3.558E+09
973	700	20.022	8111.9	575.6	3.792E+09
1023	750	20.868	8083.8	587.75	4.03E+09
1073	800	21.726		599.9	4.272E+09
1123	850	22.599		612.05	4.518E+09
1173	900	23.486		624.2	4.769E+09
1223	950	24.386		636.35	5.024E+09
1273	1000	25.3		648.5	5.283E+09
1323	1050	26.228		660.65	5.547E+09
1373	1100	27.17		672.8	5.816E+09
1423	1150	28.125		684.95	6.09E+09
1473	1200	29.094		697.1	6.369E+09
1523	1250	30.078		709.25	6.653E+09

Please cite this article in press as: A. Capriccioli, P. Frosi, Multipurpose ANSYS FE procedure for welding processes simulation, Fusion Eng. Des. (2009), doi:10.1016/j.fusengdes.2009.01.039

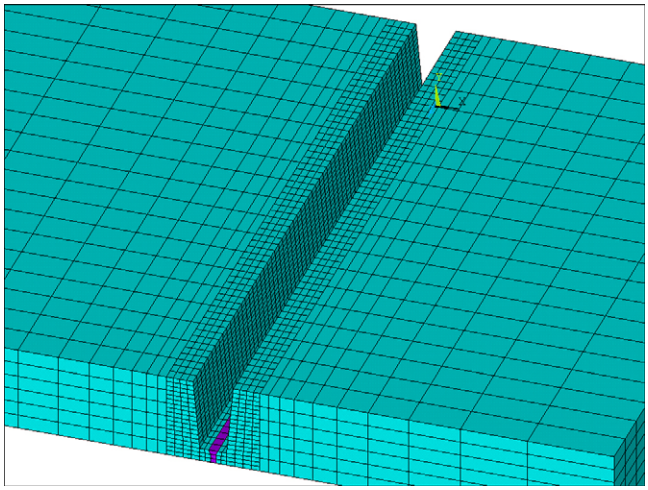

Fig. 2. Example of laser welding fem model.

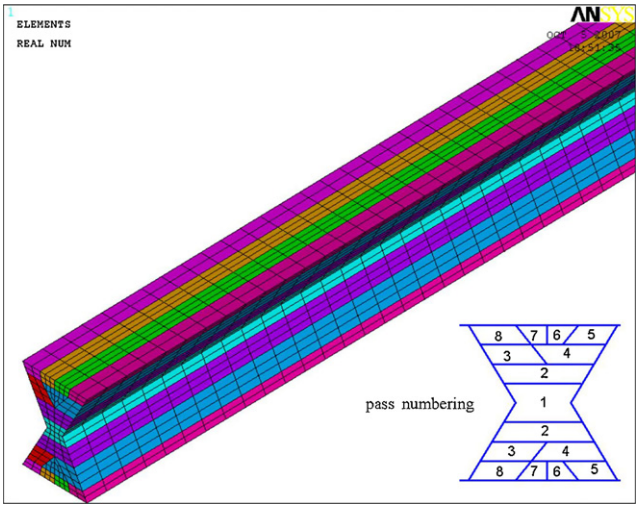

Fig. 4. Filling material elements with pass numbering.

simulate the real division, and proper contact elements are placed at the interface to avoid penetration. At the generic load step we have reactivated one "column" of elements (and at the same time the respective adjacent contact elements are "killed"); then we have loaded the model with the correspondent temperature distributions from the thermal analysis.

In the case of TIG the procedure is similar: in Fig. 3 we report ANSYS model of the TIG welding specimen of AISI 316 (W7-X); the length along the caulker is 315 mm and the width of each plate is 300 mm; we have modeled also the lateral restraints that are connected to the plates with coupling nodes DOF. The connection between regions with different mesh density, like in the case of laser welding, is obtained with contact element with the same "multi-point-constraint" option. We remember that the gap size is not uniform (ranging from 3 mm to 4.5 mm) that is the begin of the subsequent considerations.

In Fig. 4 we have the elements that simulate the filling material: these elements are collected in groups according to the different passes whose numbering is reported in the small sketch at the edge of the same figure. These elements are subjected to "birth" technique: they are killed at the beginning of the thermal analysis and then for every load step a cross-sectional "strip" of elements of a given pass, are reactivated and loaded to simulate the passage of the heat source and the filling material deposition. The mechanical analysis of TIG welding has the same approach of the laser one: but in this case we don't place any contact element to avoid penetration because now the gap is opened.

Also the heat affected zone has been considered (Fig. 5): it is represented by the elements in the finer mesh zone of the plates that are near to the caulker: these elements represent the mushy zone whose final temperatures are checked to find out if the basic material is molten during welding. These region have the same mesh density of filling material. Both the laser and the TIG models have been "coated" with surface elements (surf 151) to represent the convective heat exchange; moreover the elements at the bottom of the caulker in the laser case, and the ones representing the filling material in the TIG case, are covered with the same surface elements (with the proper options) to represent the irradiation heat exchange: these elements follow the same history of the underlying brick elements with regard to birth and death technique.

The laser analysis is related to the specimen of INCONEL 625 reported in Fig. 2: the length along the caulker is 240 mm and the width of each plate is 120 mm; the experimental test has been executed in ENEA laboratories with a Nd-YAG laser of 2 kW of power source; in Table 2 we have the thermal material property used in this case.

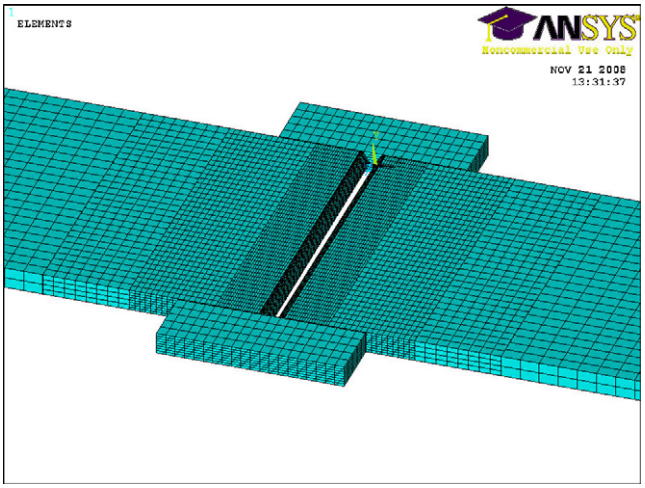

Fig. 3. Example of TIG welding fem model.

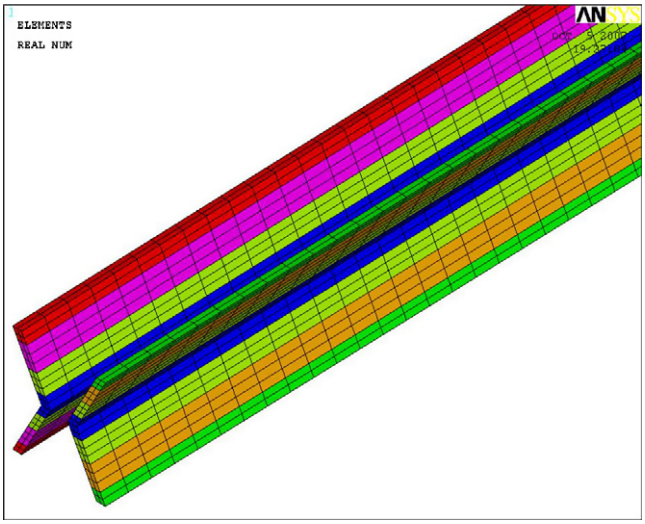

Fig. 5. Elements of heat affected zone.

Please cite this article in press as: A. Capriccioli, P. Frosi, Multipurpose ANSYS FE procedure for welding processes simulation, Fusion Eng. Des. (2009), doi:10.1016/j.fusengdes.2009.01.039

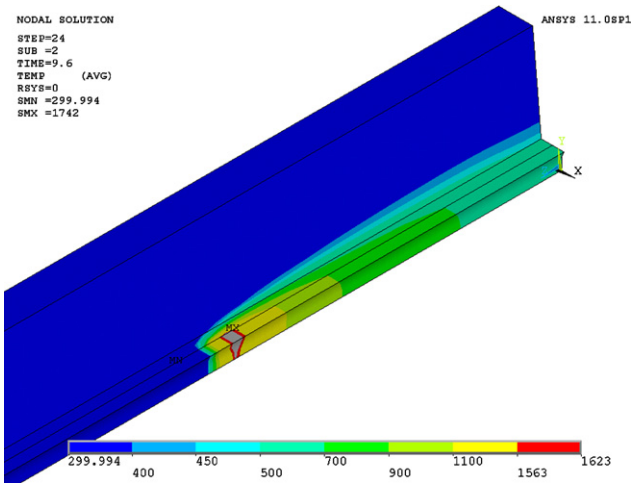

Fig. 6. Contour plot of temperature in laser welding.

In Fig. 6 we report a contour plot of thermal result along an edge of the caulker: we have chosen the scale of plot to highlight the fusion zone.

3. Sensitivity analysis

After the planning of the whole model, we can carry on several analysis on this scheme: changes in the welding speed, mesh size, material properties, developing of special procedures to minimize the calculation time etc.

This sensitivity analysis is related to the TIG tests welding process with non uniform gap named above.

A first group of analysis is related to the welding speed: keeping the same mesh size, we have performed a group of simulations with different welding speed (from 0.25 mm/sec to 10 mm/sec). You can visit the website http://www.afs.enea.it/capricci/andrea.htm, click the "numerical welding process simulation/free" button and download the Annex 1–4 of this article for viewing insightful animations.

The differences between the four cases are evident and predictable: the temperature gradients increase with the speed; obviously the powers that have been used are different because the application time is shorter when the speed increases.

If we keep constant the welding speed (2.5 mm/sec) and change the mesh size only (element length equal to ~50 mm, 25 mm, 16 mm and 10 mm, respectively 20, 40, 60 and 80 elements), we can demonstrate that for these element sizes the thermal distributions at the same time are very similar. See Annex 5 of this article in the same website mentioned above for a useful comparison.

In these simulations we have applied different procedures.

In the first method a constant *power* (not power density) is the input as Body Force Element. In this case the maximum temperature of each melted element along the welding decreases because the element size increases along the axis (gap not constant).

In the Fig. 7 it is possible to note the downward slope for every pass: moreover we can see that the absolute temperatures and the downward slope between different passes are not the same: this is because the passes have their own position, shape and boundary conditions. The first and the last temperatures of each pass can't be considered because of different thermal conditions of the respective elements.

If a constant *power density* is used as input in the Body Force Element, the maximum temperature *increases* along the axis. The reason of this "*reversal of trend*" is the change of the ratio between the net section of the "drop" (that is the cross-sectional "strip" of elements that have been reactivated at a certain load step of a given pass representing the fused filling material for that time interval) and the surface of contact with the basic material (the gap and the volume of the "drops" defined above increase but the contact surfaces with the basic material remain constant).

If the welding speed increases, the single "drop" finds different boundary conditions and the energy necessary to melt must decrease (towards adiabatic conditions). This fact is amplified by the fact that both thermal conductivity and specific heat increase with the temperature.

The second method is a fast iterative procedure: in this case the maximum temperature of the "drop" is fixed (for instance 2000 K) with the range ±5 K.

The iterative system calculates the power density necessary to reach the assigned temperature.

With this system the maximum temperature remains constant for all the passes and along each pass for all the elements, first and last ones included.

On the basis of the previous exposition, the *power density* that must be applied to each "drop" during the welding is not constant in general: indeed the gap increases but the power, as product between power density and elements volume, in this case decreases during the welding progress (curve not reported).

We have verified that the calculated values of power density keep constant the maximum temperatures per each element dur-

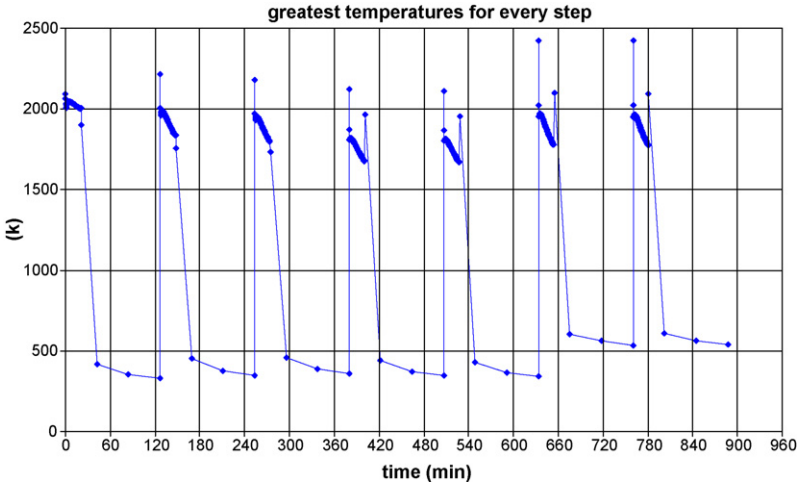

Fig. 7. Maximum temperature for all welding passes.

Please cite this article in press as: A. Capriccioli, P. Frosi, Multipurpose ANSYS FE procedure for welding processes simulation, Fusion Eng. Des. (2009), doi:10.1016/j.fusengdes.2009.01.039

ing the welding. Besides we have performed the same analysis (the fast iterative procedure) for every pass and we have found a different "power density time-history" for each pass to obtain the same maximum temperatures. It has been confirmed that all power density histories have its own "slope" and absolute values because of the different positions, shapes and boundary conditions.

Another group of analysis was related to material property sensitivity. The specific heat of the material in liquid phase was changed of ±10%. The reference maximum temperature was 1816 K and the largest variation is of 1 K; the thermal maps result identical in all cases.

In terms of largest displacements the reference case show a vertical displacement of 1.224 mm with a minimum value of 1.217 mm in case of specific heat equal to – 10%.

The thermal conductivity of the material in the full range of temperature has been changed of ±10%. The FE model and the values of temperatures are different from the previous one but the result is the same: there are no evident differences between the reference case and the others.

The last group of sensitivity analysis was related to size of the melted "drops": with the aim to decrease the calculation time, the above described model was used considering each "drop" of filling material formed of more than one transverse "strip" of elements.

A test with five axial elements for a single drop (total length about 6 mm) was performed and the results in term of powers densities and temperatures are those we expected: the power densities in the case of melted drop with five elements result lower than the other because the application time is five times longer (to maintain the same welding speed).

The maximum temperature profiles result practically identical in both cases and from the thermal results we can highlight the different lengths of the melted "drops": in the case of five elements the "tail" results more extended (plots not reported).

All these tests aim to reverse the analysis: because of the changes in heat transmission, in geometry and boundary conditions, we don't set the thermal power and then evaluate the temperature; but instead, with these models, we can predict the right sequence of thermal power to obtain a temperature established beforehand.

Finally, with the results of these sensitivity analysis we can summaries the following statements for thermal calculations:

1) the welding speed is one of the primary parameters, while the mesh size seems to have a minor effect;
2) a good analysis of the powers necessary for each pass (at fixed speed) assures the constancy of the temperatures reached during all the welding process;
3) changes of ±10% in the material properties (specific heat and thermal conductivity) seem to have negligible effects;
4) the temperature differences between each upper and lower pass result negligible with a symmetric caulker (the temperature fields result symmetric with very good approximation);
5) the time necessary for the thermal calculation is about 20 h/pass/m with 1 mm element length (Pentium 4 CPU 3 GHz; 2GB RAM). If, for example, the single "drop" is considered 5 mm length, the respective calculation time will be about 4 h/pass/m.

4. Mechanical analysis

For performing the mechanical analysis, we have chosen the kinematic hardening option in modeling the mechanical property that is we regard the elastic and plastic modulus decreasing with temperature without taking into account viscous effects. We have decided to neglect the viscous effect because the only proven data that we have near to the fusion temperature, are the one coming from the ITER database (Tables 3 and 4) and we are not very confident about parameter to use in any viscous constitutive models. The convergence's problems coming from the small plastic modulus at high temperature can be overcome using the shorter elements as possible (1.3 mm) and consider the situation of multiple (five) axial elements for a single drop (see above). In Fig. 8 there is a contour plot of total displacement in the TIG welding test at the end of the second upper pass. In Fig. 9 there is the same contour plot in the case of laser welding after the cooling period and the restraint's removal: this numerical result agrees the experimental observation that the sample remains almost plane at the end of the experience.

The calculation time depends on the model size, the geometry etc., but is about 4–5 times longer than the thermal one: so we have developed a special procedure in the case of mechanical analysis of

Table 3
AISI 316 mechanical material property.

Temperature (K)	Yield Strength (N/m^2)	Tensile Strength (N/m^2)	Elastic Modulus (N/m^2)
273	3.47E+08	6.45E+08	2.00E+11
293	3.20E+08	6.20E+08	1.96E+11
373	2.11E+08	5.20E+08	1.92E+11
423	1.89E+08	4.90E+08	1.88E+11
473	1.67E+08	4.60E+08	1.84E+11
523	1.56E+08	4.50E+08	1.80E+11
573	1.45E+08	4.40E+08	1.76E+11
623	1.40E+08	4.30E+08	1.72E+11
673	1.35E+08	4.20E+08	1.68E+11
723	1.32E+08	4.10E+08	1.64E+11
773	1.29E+08	4.00E+08	1.60E+11
823	1.26E+08	3.90E+08	1.56E+11
873	1.23E+08	3.80E+08	1.52E+11
923	1.20E+08	3.70E+08	1.48E+11
973	1.17E+08	3.60E+08	1.44E+11
1023	1.14E+08	3.50E+08	1.39E+11
1073	1.11E+08	3.40E+08	1.35E+11
1123	1.08E+08	3.30E+08	1.31E+11
1173	1.05E+08	3.20E+08	1.27E+11
1223	1.02E+08	3.10E+08	1.23E+11
1273	9.90E+07	3.00E+08	1.19E+11
1323	8.80E+07	2.82E+08	1.12E+11
1373	6.60E+07	2.54E+08	1.05E+11
1423	4.30E+07	2.11E+08	9.44E+10
1473	2.40E+07	9.80E+07	2.00E+10
1523	1.35E+07	6.00E+07	1.17E+10
1573	1.05E+07	3.90E+07	7.00E+09
1623	1.00E+07	2.70E+07	5.56E+09

Table 4
INCONEL 625 mechanical material property.

Temperature (K)	Yield strength (Pa)	Tensile strength (Pa)	Elastic modulus (Pa)
273	3.75E+08	1.44E+09	1.97E + 11
323	3.49E+08	1.41E+09	1.94E + 11
373	3.26E+08	1.38E+09	1.91E + 11
423	3.06E+08	1.35E+09	1.86E + 11
473	2.90E+08	1.32E+09	1.82E+11
523	2.77E+08	1.30E+09	1.78E+11
573	2.67E+08	1.28E+09	1.75E+11
623	2.60E+08	1.27E+09	1.73E+11
673	2.56E+08	1.26E+09	1.72E+11
723	2.54E+08	1.25E+09	1.71E+11
773	2.54E+08	1.25E+09	1.70E+11
823	2.53E+08	1.25E+09	1.70E+11
873	2.51E+08	1.26E+09	1.69E+11
923	2.47E+08	1.27E+09	1.66E+11
973	2.39E+08	1.28E+09	1.60E+11
1023	2.25E+08	1.30E+09	1.51E+11
1073	2.05E+08	1.32E+09	1.36E+11
1123	1.74E+08	1.34E+09	1.16E+11
1173	1.32E+08	1.37E+09	8.73E+10
1273	9.50E+07	1.30E+08	8.70E+10
1473	3.50E+07	3.60E+07	5.30E+10

Please cite this article in press as: A. Capriccioli, P. Frosi, Multipurpose ANSYS FE procedure for welding processes simulation, Fusion Eng. Des. (2009), doi:10.1016/j.fusengdes.2009.01.039

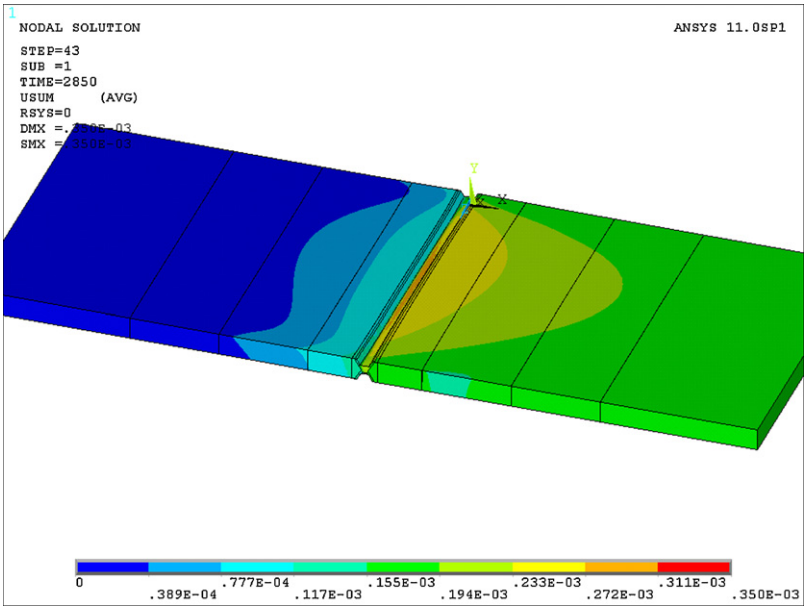

Fig. 8. Contour plot of total displacement in a TIG welding.

TIG welding (because is the most time demanding) for obtaining a solution that results conservative with respect to the real one.

At first we have performed the entire mechanical analysis, then we have selected the nodes relative to the filling material and relative to the region very near to the caulker; then we have stored their displacements in the shrinkage direction. Practically we have two sets: the first one is relative to the displacements of the nodes near to the caulker and that belong to the clamped plate (finer mesh region of the left plate in Fig. 3); they result in a band around zero value (the two upper bands of the graph in Fig. 10). The second one is relative to the nodal displacements of filling material and the nodes near to the caulker and that belong to the other plate simply supported (finer mesh region of the right plate and filling material in Fig. 3). The nodal displacements of this second set, that really represent the shrinkage, are represented by the two lower bands of the graphs in Fig. 10: this graph is not related to a specific position but it is a result for all the nodes belonging to the two sets mentioned above at the end of a given pass (after the second upper and lower passes); for the other passes the graphs are similar. These set of result is a sort of a reference case.

After that we have performed a distinct mechanical analysis for every pass (we will call this case “pseudo-linear approach”): the first one is related to the root pass and is equal to that of the previous case; the other analysis are related to the corresponding other passes but they have been executed beginning from the configuration of their own previous pass (with the respective elements reactivated), but with initial zero stress and strain. The respective average values of shrinkage displacement for each pass is grater than that obtained in the real case because the material starts from a free-stress state and it has no deformation energy accumulated. In Fig. 11 we plot the subsequent average displacements for all passes in the total elastic-plastic approach and pseudo-linear one.

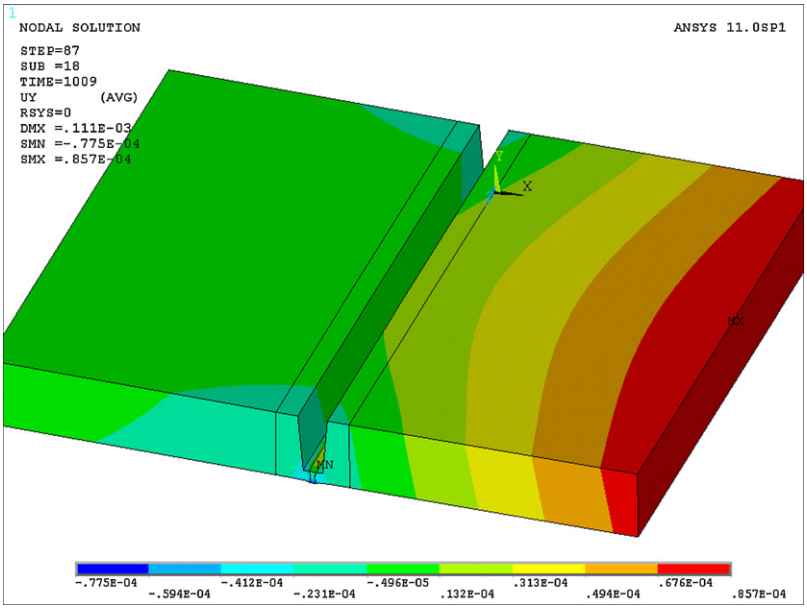

Fig. 9. Contour plot of vertical displacement in a laser welding.

Please cite this article in press as: A. Capriccioli, P. Frosi, Multipurpose ANSYS FE procedure for welding processes simulation, Fusion Eng. Des. (2009), doi:10.1016/j.fusengdes.2009.01.039

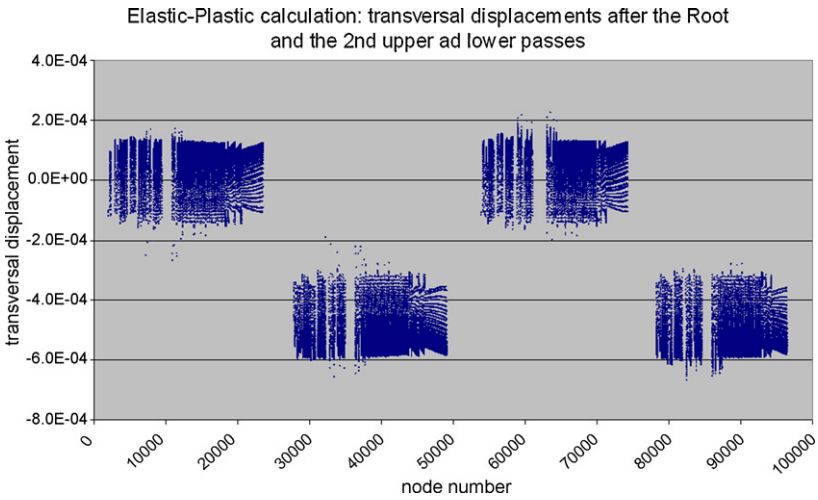

Fig. 10. Transverse nodal displacement after two passes.

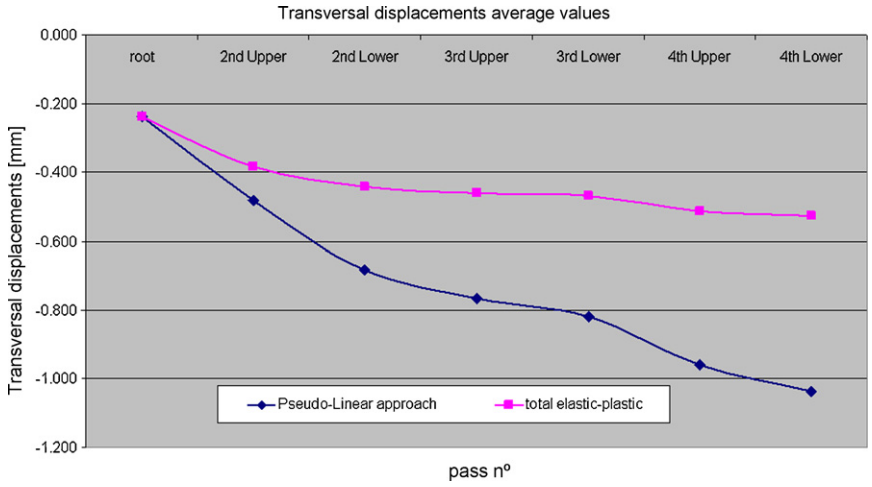

Fig. 11. Average displacement for "pseudo-linear" and elastic–plastic analysis.

In Fig. 12 we plot the contribution of every pass in the same two cases: we observe that the greatest contribution to the global displacement is given in the early passes; then when the caulker is going to fill, the resistant section increases and the additional thermal loads does not add further great strains. We can see immediately that "pseudo-linear" approach is conservative: it allows to overestimate the final displacement. Conscious of this fact, the pseudo-linear approach can be used to reduce the calculation time:

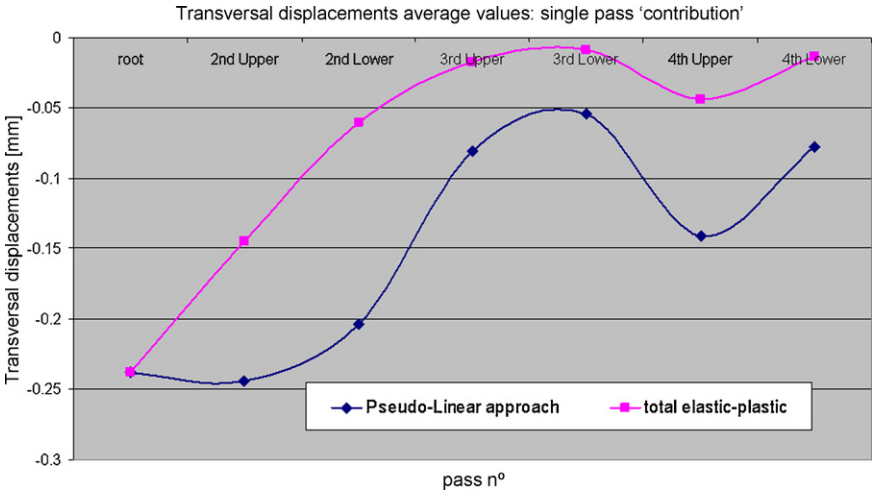

Fig. 12. Single contribution of average displacement for every pass.

Please cite this article in press as: A. Capriccioli, P. Frosi, Multipurpose ANSYS FE procedure for welding processes simulation, Fusion Eng. Des. (2009), doi:10.1016/j.fusengdes.2009.01.039

indeed it is possible (after performing the "ordinary" thermal analysis) to execute *at the same time* a set of mechanical analysis as much as the number of passes and then simply add the contribution of each pass.

5. Conclusions

A fem method has been explained to analyze laser and TIG welding. The birth and death technique has been adopted and material property can be simulated till to the fusion state. An iterative procedure that assures a fixed maximum temperature along the single pass has been developed. In order to reduce the computer time a simplified procedure has been developed in the case of TIG welding mechanical analysis: this procedure lets to run the whole welding mechanical simulation with a considerable saving in computer time. The next pass of this analysis is to think about a procedure that could reduce the overestimation involved in this simplified analysis. Moreover this simplified analysis must be verified with other geometries other than the plane one.

Also this simplified approach is trustworthy only if we are interested in displacements of the welding joint: if we want to predict the state of stress (elastic or plastic), further theoretical thought in the comparison with the real case are needed.

References

[1] E. Friedman, Thermomechanical analysis of the welding process using the finite element method, ASME J. Pressure Vessel Technol. 97 (1975) 206–212.
[2] C.T. Karlsson, B.L. Josefson, Three-dimensional finite element analysis of temperatures and stresses in a single-pass butt-welded pipe, ASME J. Pressure Vessel Technol. 112 (1990) 76–84.
[3] P. Dong, F. Brust, Welding residual stresses and effects in fracture in pressure vessel and piping components: a millennium review and beyond, ASME J. Pressure Vessel Technol. (2000) 329–338 (the millennium issue 122).
[4] L. Borjesson, L. Lindgren, Simulation of multipass welding with simultaneous computation of material properties, J. Eng. Mater. Technol. 123 (2001) 106–111.
[5] S. Qingyu, L. Anli, Z. Haiyan, W. Aiping, Development and application of the adaptive mesh technique in the three-dimensional numerical simulation of the welding process, J. Mater. Process. Technol. 121 (2002) 167–172.
[6] Carmignani B., Toselli G., Visparelli D., Bonifazio M., Sangiorgi S., Trestini D. et al, Numerical simulation of the Welds for the Components of Plasma Chamber of Ignitor Fusion Machine, ENEA RT/2007/33/FIM.

Please cite this article in press as: A. Capriccioli, P. Frosi, Multipurpose ANSYS FE procedure for welding processes simulation, Fusion Eng. Des. (2009), doi:10.1016/j.fusengdes.2009.01.039